1998

Ion Bernstein Waves Driven by Two Transverse Flow Layers

Mark Anthony Reynolds
Embry-Riddle Aeroautical University, reynoldb2@erau.edu

G. Ganguli
Naval Research Laboratory, Washington, D.C.

Ion Bernstein waves driven by two transverse flow layers

M. A. Reynolds[a] and G. Ganguli
Beam Physics Branch, Plasma Physics Division, Naval Research Laboratory, Washington, D.C. 20375

(Received 9 February 1998; accepted 16 April 1998)

The interaction between two narrow layers of $\mathbf{E}\times\mathbf{B}$ flow is investigated, along with their stability properties. The mode frequencies, growth rates, and eigenfunctions are calculated. It is found that the instability due to a single layer is robust to the inclusion of a second layer. Specifically, when the separation between the layers is on the order of the ion-cyclotron radius, there is strong coupling between the two layers and the second layer is destabilizing. In addition, when the flow velocities are in opposite directions a wide variety of modes is possible, including near-zero-frequency modes, resulting in broadband structure in both the frequency spectrum and the wave number spectrum. These results may have implications for the understanding of the auroral ionosphere, where such spatial structure in the transverse electric field is often observed. © *1998 American Institute of Physics.* [S1070-664X(98)03807-5]

I. INTRODUCTION

Nonuniformities in the direction perpendicular to the magnetic field are routinely observed in a variety of plasmas. The complicated structure in the density, current, and electric field of the auroral ionospheric environment[1] is one striking example. For many years, observations of the auroral ionosphere[2–4] have revealed fine scale structure in the transverse electric field, in which the overall effect is one of strong velocity shear, resembling many individual $\mathbf{E}\times\mathbf{B}$ flow layers in close proximity. In addition, laboratory experiments[5,6] designed to model the space environment have been able to externally drive electric fields of this type. The linear stability properties of waves in such nonuniform media are difficult to predict *a priori*: each situation must be studied individually, and evaluated on a case-by-case basis. In this paper, we study the effects that structured, nonuniform $\mathbf{E}\times\mathbf{B}$ flow has on the stability of ion Bernstein waves. Specifically, we investigate the case of two layers (whose thickness L is on the order of the ion-cyclotron radius, $L \gtrsim \rho_i$) with finite $\mathbf{E}\times\mathbf{B}$ flow, immersed in a background plasma that is stationary.

It has been shown, both theoretically[7,8] and experimentally,[9,10] that a single localized flow layer (with its associated velocity shear) can be unstable to ion-cyclotron-like waves. In the frame of the background plasma the electrostatic wave energy density is negative within the flow layer and positive outside the flow layer, which means that a loss of wave energy from the layer can sustain wave growth.[7] The waves that grow must propagate energy outward across the boundary between the layer and the background plasma. Analysis of single-particle orbits[11] in the field structure generated by the instability shows that ions fall through a potential drop and give up this energy to the wave, similar to the physical mechanism of a magnetron. In this paper, we generalize the single-layer results to include the new effects due to the addition of a second layer. Because an examination of the field structure is crucial to the understanding of the physics of this instability, we use the eigenfunctions of the wave potential in a given flow structure as an important pedagogical tool. Of course, the eigenfunctions may not be orthogonal if the system exhibits transient behavior, and other methods must be used to deduce the linear response.[12] This complication is not considered here.

The eigenvalue equation for ion Bernstein waves in a nonuniform plasma is derived in Sec. II, the dispersion relation for our choice of geometry is given in Sec. III, and relevant results for a single flow layer are described in Sec. IV. In Secs. V and VI we investigate in detail two types of structures that are generic in character. The first type, Sec. V, is characterized by flows in the same direction, with a region of zero velocity separating the two layers. The second type, Sec. VI, is characterized by flows in opposite directions with no separation between the two layers (this approximates a so-called ''paired electrostatic shock'' [2]). Section VII is the conclusion.

II. ION BERNSTEIN WAVES IN NONUNIFORM PLASMAS

To obtain electrostatic ion Bernstein waves,[13] we make the usual approximations of low frequency ($\omega \ll \Omega_e$, where Ω_e is the electron-cyclotron frequency), long perpendicular wavelength ($k_\perp \rho_e \ll 1$, where ρ_e is the electron-cyclotron radius), and perpendicular propagation ($k_\parallel \equiv 0$; finite $k_\parallel$ introduces Landau damping, which is ignored here). In addition, we assume $\omega_{pi} \gg \Omega_i$ (where ω_{pi} and Ω_i are the ion-plasma and ion-cyclotron frequencies), which holds for most plasmas of interest. This is equivalent to restricting the frequency regime to well below the lower hybrid frequency, $\omega \ll \omega_{lh}$. Under these approximations, and taking magnetic field to be in the z direction, the electrostatic dispersion relation for a uniform plasma has the simple form[13]

[a]National Research Council–NRL Research Associate. Electronic mail: anthony@ppdu.nrl.navy.mil

$$\mathscr{D}=1-\sum_n \Gamma_n(b_\perp)\,\frac{\omega}{\omega-n\Omega_i}=0, \tag{1}$$

where $b_\perp=(k_x^2+k_y^2)\rho_i^2/2$, $\rho_i=\overline{v_i}/\Omega_i$ is the ion-cyclotron radius, $\overline{v_i}=\sqrt{2T_i/m_i}$ is the ion thermal velocity, $\Gamma_n(b_\perp)=\exp(-b_\perp)I_n(b_\perp)$, and I_n is a modified Bessel function. The solution of Eq. (1) gives the so-called ''pure'' ion Bernstein waves.[14]

When the plasma is nonuniform, an exact solution of the plasma response requires an integral-differential formulation.[15] To lowest order, however, nonuniformities in the x direction can be included by expanding $\mathscr{D}$ for small k_x, and making the substitution $k_x\rightarrow -i\partial/\partial x$. (Here, we have assumed that any nonuniformities in the y and z directions are negligible compared with those in the x direction.) The uniform dispersion relation then becomes a second order differential (eigenvalue) equation

$$\left\{\mathscr{D}\Big|_{k_x=0}-\left(\frac{\partial\mathscr{D}}{\partial(k_x^2)}\right)_{k_x=0}\frac{\partial^2}{\partial x^2}\right\}\phi(x)=0, \tag{2}$$

where ϕ is the electrostatic potential, and the quantities inside the braces ($\mathscr{D}$ and its derivative) are to be evaluated for $k_x=0$. When the plasma parameters are piecewise constant, the general solution to Eq. (2) in each region is an exponential, $\phi(x)\sim\exp(\pm i\mathsf{k}x)$, where

$$\mathsf{k}^2=-\frac{\mathscr{D}}{\partial\mathscr{D}/\partial(k_x^2)}\Big|_{k_x=0}$$

$$=\frac{1-\Sigma_n\Gamma_n(b)\tilde{\omega}/(\tilde{\omega}-n\Omega_i)}{(\rho_i^2/2)\Sigma_n\Gamma_n'(b)\tilde{\omega}/(\tilde{\omega}-n\Omega_i)}, \tag{3}$$

$b=k_y^2\rho_i^2/2$, $\Gamma'=d\Gamma/db$, $\tilde{\omega}=\omega-k_yV_E(x)$, and $\mathbf{V}_E(x)=-\hat{\mathbf{y}}cE_x(x)/B$. The quantity $\tilde{\omega}$ is the Doppler-shifted frequency due to the $\mathbf{E}\times\mathbf{B}$ flow, and is a function of position in this case. (In previous work,[5–11,15,16] the symbol ω_1 has been used to denote $\tilde{\omega}$.) The quantity ω has both a real and imaginary part, which we denote $\omega\equiv\omega_r+i\gamma$, where ω_r is the frequency and γ is the growth rate.

III. GEOMETRY AND NONLOCAL DISPERSION RELATION

We consider two layers, labeled layer 1 and layer 2, with widths L_1 and L_2 and flow velocities V_1 and V_2, separated by a distance Δ. The $\mathbf{E}\times\mathbf{B}$ drift velocity as a function of x is specified in five different regions

$$V_E=\left\{\begin{array}{ll} 0 & x<-L_1/2 \\ V_1 & -L_1/2<x<L_1/2 \\ 0 & L_1/2<x<L_1/2+\Delta \\ V_2 & L_1/2+\Delta<x<L_1/2+\Delta+L_2 \\ 0 & L_1/2+\Delta+L_2<x \end{array}\right\}. \tag{4}$$

The geometry is sketched in Fig. 1. A piecewise constant flow velocity is chosen for its simplicity, and because the instability of interest does not depend explicitly on gradients in the flow, but does depend on the global nonuniformity.[8]

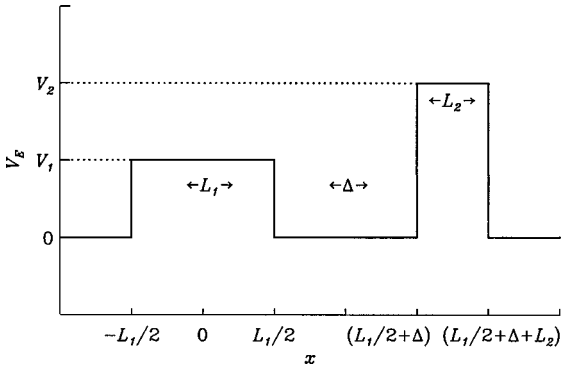

FIG. 1. Geometry of the structured flow. The two layers have widths L_1 and L_2, flow velocities V_1 and V_2, and are separated by a distance Δ.

The nonlocal dispersion relation for this nonuniform plasma is obtained by matching both ϕ and $\partial\phi/\partial x$ across the four boundaries between the five regions (see the Appendix for details and a generalization to an arbitrary number of layers). The two-layer dispersion relation can be written as a product of two single-layer dispersion relations plus a coupling term

$$D_{12}^{(2)}\equiv D_1^{(1)}D_2^{(1)}+C_{12}=0. \tag{5}$$

The superscript indicates the number of layers and the subscripts label each layer. That is,

$$D_1^{(1)}\equiv(\mathsf{k}_0-\mathsf{k}_1)^2e^{i\mathsf{k}_1L_1}-(\mathsf{k}_0+\mathsf{k}_1)^2e^{-i\mathsf{k}_1L_1}=0 \tag{6}$$

is the nonlocal dispersion relation for layer 1 (i.e., assuming $V_2=0$), $D_2^{(1)}$ is identical in form to $D_1^{(1)}$ with $\mathsf{k}_1\rightarrow\mathsf{k}_2$ and $L_1\rightarrow L_2$, and

$$C_{12}=4e^{2i\mathsf{k}_0\Delta}(\mathsf{k}_0^2-\mathsf{k}_1^2)(\mathsf{k}_0^2-\mathsf{k}_2^2)\sin(\mathsf{k}_1L_1)\sin(\mathsf{k}_2L_2) \tag{7}$$

is the coupling between the two layers. The wave numbers in the x direction in the flow layers, k_1 and k_2, are given by Eq. (3) with $\tilde{\omega}$ replaced by $\omega-k_yV_1$ and $\omega-k_yV_2$, while the wave number in the regions with no flow, k_0, is given by Eq. (3) with $\tilde{\omega}$ replaced by ω.

The dispersion relation for a single layer, $D_1^{(1)}=0$, can be factored into terms responsible for definite parity (even and odd) eigenfunctions

$$D_1^{(1)}=4[\mathsf{k}_0\cos(\mathsf{k}_1L_1/2)-i\mathsf{k}_1\sin(\mathsf{k}_1L_1/2)]$$

$$\times\{i\mathsf{k}_0\sin(\mathsf{k}_1L_1/2)-\mathsf{k}_1\cos(\mathsf{k}_1L_1/2)\}=0, \tag{8}$$

where the eigenfunctions associated with the eigenvalues of the term in square brackets are even in x, while those associated with the term in curly braces are odd. No such factoring is possible in the more general case considered here because the flows do not exhibit any inherent symmetry in x.

The result in Eq. (8) is equivalent to the solution of the time-independent Schrödinger equation for a finite square well, and Eqs. (5)–(7) show the extension from a single square well to two square wells. We have expressed the result in a form that separates the interaction between the two flow layers (or square wells) from the dynamics of a single flow layer. Equation (7) shows that the coupling between the two layers is proportional to $\exp(-2\Delta\,\mathrm{Im}\,\mathsf{k}_0)$ which means that for large Δ the layers are uncoupled (of course, the fact

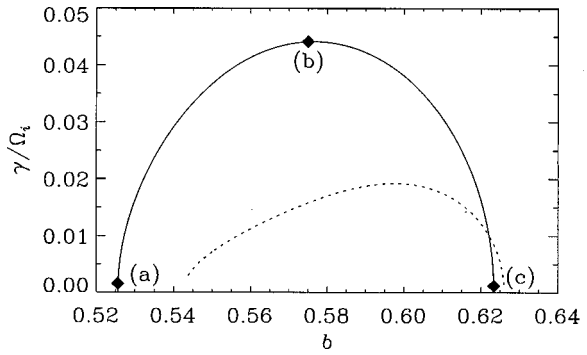

FIG. 2. Growth rate for a single layer as a function of wave number b for two different thicknesses, $L_1=3\rho_i$ (solid) and $L_1=6\rho_i$ (dotted). The flow velocities are $V_1=3\overline{v_i}$ and $V_2=0$. The three diamonds (a)–(c) mark eigenvalues for which the eigenfunctions are shown in Fig. 3.

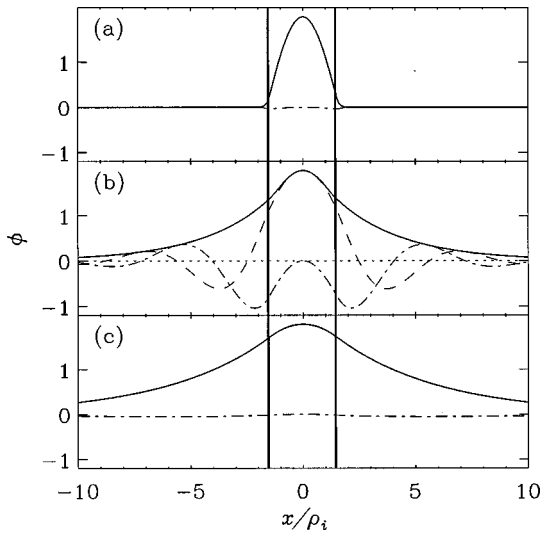

FIG. 3. Eigenfunctions for a single layer of thickness $L_1=3\rho_i$ and flow velocity $V_1=3\overline{v_i}$ for three different values of b: (a) $b=0.52559$, (b) $b=0.575$, (c) $b=0.62336$. The dashed line is Re ϕ, the dot-dashed line is Im ϕ, and the solid line is $|\phi|$. The two vertical lines delineate the edges of the layer, and the dotted line in (b) marks the zero value. In (c), Re ϕ and $|\phi|$ are virtually identical.

that Im k_0 is positive is required by the boundary condition that $\phi\to 0$ for $|x|\to\infty$). In this case, the modes of one layer are normal modes of the system regardless of the other layer. If the layers are identical, then there is the possibility that some roots are degenerate. When $\Delta \lesssim 1/(2\ \mathrm{Im}\ k_0)$ (the case we wish to investigate here), the coupling between the layers is strong, and the normal modes are global in nature and incorporate the physics of the interaction of the two layers.

IV. SINGLE-LAYER RESULTS OF RELEVANCE

When $V_2=0$ (i.e., $k_2=k_0$), the dispersion relation is given by Eq. (8) and the resulting stability properties have been discussed elsewhere in detail (see Ganguli[8] and references therein). We describe briefly only the results relevant to the two-layer case. This includes a detailed look at the properties of the eigenfunctions, which form the basis for our interpretation of the physics in the two-layer case.

We choose a coherent mode,[7] where the growth rate is positive only in a narrow range of b. (The ion-cyclotron radius ρ_i is held constant, so that a variation of b signifies a variation of k_y.) Figure 2 shows γ as a function of b for a single layer, with flow velocity $V_1=3\overline{v_i}$. (The frequency, ω_r, is not shown as it remains approximately equal to $1.6\Omega_i$ over the entire range of b.) Two different widths are shown, $L_1=3\rho_i$ and $L_1=6\rho_i$. This illustrates the property that as the width increases, the growth rate decreases. Physically, the reason is that the velocity shear is weaker. In the next section it will be shown that when the separation between two layers is small, they can either be strongly coupled or act as essentially a single, wider, layer (with a corresponding reduction in the growth rate), depending on the wave number.

A heuristic derivation of the growth rate, which considers only energy flow, results in[15]

$$\gamma=-\frac{v_g U_0}{L_1 U_1}, \tag{9}$$

where v_g is the group velocity in the x direction across the boundaries of the layer ($x=\pm L_1/2$), U_0 is the electrostatic wave energy density in the region of no flow outside the layer, and U_1 is the electrostatic wave energy density inside the layer. When U_1 is negative, U_0 is positive, and v_g is positive, which is the case here, there is the possibility for instability. (Positive v_g means the group velocity points away from the layer.)

This energy flow can be inferred from Fig. 3 where the eigenfunctions $\phi(x)$ for a single layer of width $L_1=3\rho_i$ are shown for three different values of b (corresponding to the diamonds in Fig. 2). When γ is maximum [Fig. 3(b)], energy propagates away from the layer in both directions. This is the physical mechanism by which the instability grows: because the electrostatic wave energy density is negative within the layer and positive outside the layer, the eigenfunction must be a wave whose group velocity propagates energy across the boundary between the layer and the background plasma in order for the free energy to be released. The direction of energy flow is determined from Fig. 3(b) and the fact that these waves are backward waves. In Fig. 3(b), the phase of Re ϕ lags that of Im ϕ by 90°, which means that the phase velocity points toward the layer. In addition, for frequencies below the lower hybrid frequency, ion Bernstein waves are backward waves for all values of $k_\perp$. (This can be seen from Fig. 1 of Ref. 14 by noting that $d\omega/dk_\perp<0$.) These two facts together indicate that the group velocity points away from the layer, thus satisfying the criteria for instability given in Eq. (9). When the eigenfunction is either localized within the layer [Fig. 3(a)] or evanescent outside the layer [Fig. 3(c)] the growth rate is reduced. Only the ''ground state'' eigenfunctions (and eigenvalues) are shown, because they typically have the largest growth rates. Similar to the quantum square well problem, however, there are other ''bound states,'' and they exhibit the same physical behavior just described for the ground state.

This physical behavior exists for two layers as well, but the possibility of coupling between the layers, and the resulting interference between the eigenfunctions associated with

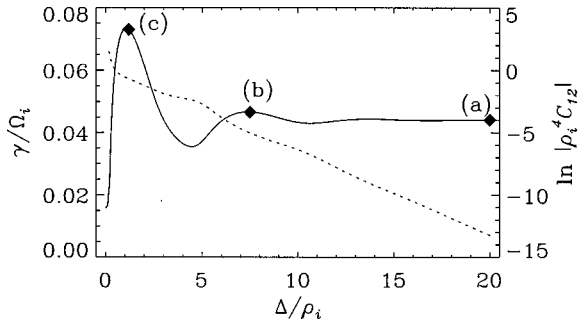

FIG. 4. Growth rate (solid line) and coupling term (dotted line) for two identical layers as a function of separation Δ. The thicknesses are $L_1=L_2=3\rho_i$, the flow velocities are $V_1=V_2=3\overline{v_i}$, and the wave number is $b=0.575$. The three diamonds (a)–(c) mark eigenvalues for which the eigenfunctions are shown in Fig. 5.

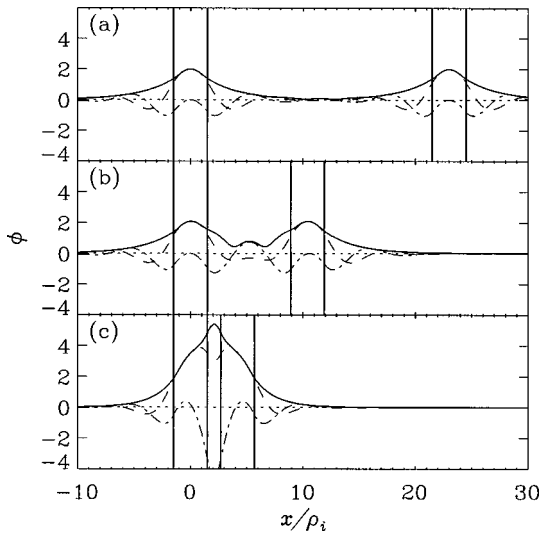

FIG. 5. Eigenfunctions for two layers of thickness $L_1=L_2=3\rho_i$ and flow velocities $V_1=V_2=3\overline{v_i}$ for three different values of Δ: (a) $\Delta=20\rho_i$, (b) $\Delta=7.5\rho_i$, (c) $\Delta=1.2\rho_i$. The dashed line is Re ϕ, the dot-dashed line is Im ϕ, and the solid line is $|\phi|$, and $b=0.575$. The vertical lines delineate the edges of the layers, and the dotted lines mark the zero values.

each layer, results in new effects with corresponding qualitative and quantitative changes in the mode structure and growth rates.

V. IDENTICAL LAYERS

We now turn to the first of the two generic structure types: two identical layers. Identical layers are chosen because we want to focus on the physics of the coupling mechanism, and the behavior of the coupling term C_{12}. This can be illustrated most easily when $D_1^{(1)}$ and $D_2^{(1)}$ are identical. When the two layers are widely separated, the normal modes will be similar to those of a single layer, with similar stability properties. As the separation decreases, however, the coupling term C_{12} plays a nontrivial role.

There are two parameters which quantify the strength and behavior of the interaction between the two layers. The first parameter is a measure of the strength of the coupling,

$$\delta \equiv 2\Delta \ \mathrm{Im}\ \mathsf{k}_0. \tag{10}$$

The coupling term, C_{12}, is proportional to $\exp(-\delta)$, so that for large δ (large separations) the coupling is exponentially small. In addition, $\delta/2$ is the number of e-foldings of the amplitude of the eigenfunction between the layers. In the region of no flow between the layers, the eigenfunction, ϕ, is proportional to $\exp(-x\ \mathrm{Im}\ \mathsf{k}_0)$. Evaluating this for a separation of $x=\Delta$ results in $\exp(-\delta/2)$. This is consistent with the physical idea that C_{12} should have the same dependence on separation as $\phi\phi^*$, a measure of the energy. The second parameter is the number of wavelengths that fit between the layers

$$N \equiv \frac{\Delta}{\lambda_x} = \frac{\Delta\ \mathrm{Re}\ \mathsf{k}_0}{2\pi}, \tag{11}$$

where λ_x is the wavelength in the x direction in the region between the layers.

To illustrate how these parameters determine the interaction, we choose $L_1=L_2=3\rho_i$ and $V_1=V_2=3\overline{v_i}$. Figure 4 shows the growth rate in the transition between large and small separation, for $b=0.575$. Also shown is the magnitude of the coupling term C_{12}, which decays exponentially with increasing separation Δ. Three regimes can be distinguished. For large separations, $\Delta \gtrsim 20\rho_i$, the coupling term is exponentially small, and in this limit a root of the single layer $D_1^{(1)}$ is also a (degenerate) root of $D_{12}^{(2)}$. The physics of this limit was discussed in the previous section. For intermediate separations, $5\rho_i \lesssim \Delta \lesssim 20\rho_i$, the growth rate oscillates with Δ. Finally, for small separations, $\Delta \lesssim 5\rho_i$, C_{12} becomes appreciable, the coupling between the two layers is strongest, and the growth rate approaches twice its single layer value. (As in the single-layer case, $\omega_r \approx 1.6\Omega_i$ for all values of Δ.) This behavior can be understood by examining the eigenfunctions.

The eigenfunctions for three separations ($\Delta/\rho_i = 20, 7.5, 1.2$) are shown in Fig. 5. For large separations, Fig. 5(a), each layer drives waves locally, independent of the other layer. For this case, $\delta \approx 13$, which means that the two layers are effectively uncoupled. Of course, any noise in the plasma will destroy the slight coupling that exists theoretically for these large separations. As the separation decreases, the coupling increases, and the growth rate changes from its single-layer value and oscillates with Δ. These oscillations are due to an integral number of wavelengths fitting in the potential well between the layers, as given by the parameter N. This can be seen from Fig. 6, which shows N as a function of layer separation. (For comparison, the growth rate is also shown.) When N is an integer, the growth rate is near a maximum. This is similar to the effect that N has on the transmission coefficient through two quantum square wells. The growth rate is not exactly a maximum, however, because the effective potential well between the layers is not infinite. The eigenfunction for the separation where $N \approx 1$ is shown in Fig. 5(b). When $\Delta \lesssim 5\rho_i$, the waves generated by each layer constructively interfere, as shown in Fig. 5(c), and the eigenfunction is largest in the region between the two layers. This is because the waves propagating away from each layer are reflected multiple times in the region between the layers. In

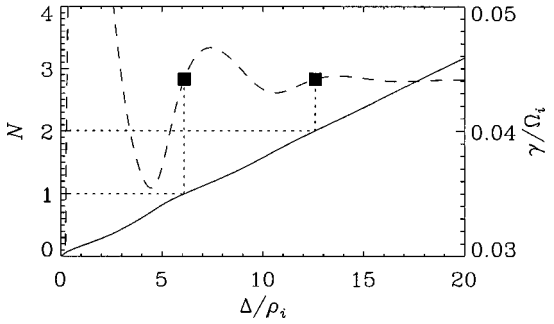

FIG. 6. Number of wavelengths N that fit between the layers (solid line), for $L_1=L_2=3\rho_i$, $V_1=V_2=3\overline{v_i}$, and $b=0.575$. Also shown is the growth rate (dashed line). The dotted lines indicate the values of the separation for which an integral number of wavelengths fit between the layers. The squares indicate the growth rate for these separations.

this regime, there is no simple formula (e.g., an integral number of wavelengths) which will predict the separation with maximum γ.

This coupling can be investigated in more detail by looking at the behavior of γ (and the eigenfunctions) as a function of b. Figure 7 shows $\gamma(b)$ for two values of the separation $(\Delta/\rho_i=0.12,1.2)$. The growth rates for a single layer of widths $L_1=3\rho_i$ and $L_1=6\rho_i$ are shown for comparison. Figure 8 shows the eigenfunctions corresponding to the three diamonds in Fig. 7. For case (a), the two layers are essentially uncoupled: the growth rate is close to the single-layer value, the eigenfunction is localized, $\delta\approx 4.5$ and $N\approx 1.5$, which means that the spatial damping in the x direction is strong enough for the distance between the layers to be effectively large. For case (c), the two close layers behave as a single wide layer: the growth rate is low, the eigenfunction is evanescent outside the layers, $\delta\approx 0.4$, and $N\approx 0.06$, which is small enough that the eigenfunction is not affected by the narrow potential well between the two layers. In the intermediate regime of enhanced growth rate, where the eigenfunction is shown in Fig. 8(b), the coupling is very strong and the system behaves neither like two separate single narrow layers nor one single wide layer.

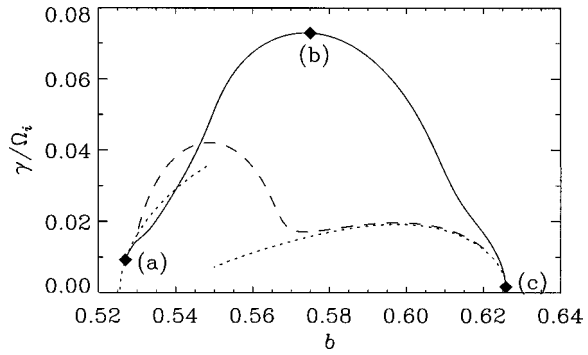

FIG. 7. Growth rate for two identical layers as a function of b, for two values of the separation $\Delta/\rho_i=0.12$ (dashed), 1.2 (solid). For comparison, the dotted lines show the growth rates of a single layer of widths $L_1=3\rho_i$ and $L_1=6\rho_i$ (see Fig. 2). The three diamonds (a)–(c) mark eigenvalues for which the eigenfunctions are shown in Fig. 8.

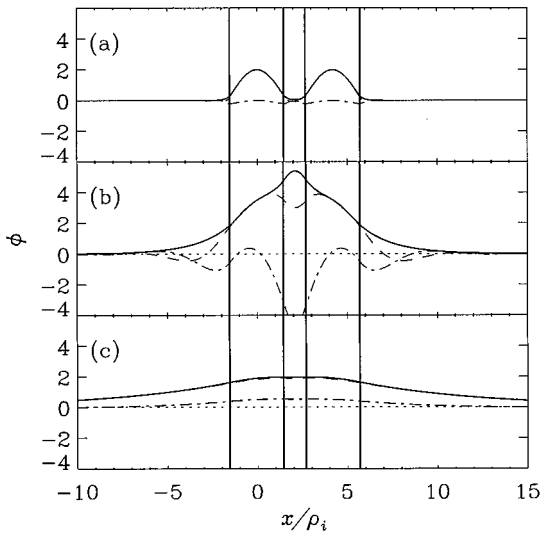

FIG. 8. Eigenfunctions for two layers of thickness $L_1=L_2=3\rho_i$ and flow velocities $V_1=V_2=3\overline{v_i}$ separated by a distance $\Delta=1.2\rho_i$ for three different values of b: (a) $b=0.527$, (b) $b=0.575$, (c) $b=0.62582$. The dashed line is Re ϕ, the dot-dashed line is Im ϕ, and the solid line is $|\phi|$. The vertical lines delineate the edges of the layers, and the dotted lines in (b) and (c) mark the zero values.

Maximum Growth Rate

The results so far have been presented for specific values of b. In the asymptotic limit, however, the plasma will respond most strongly to the wave number component with the largest growth rate. It is important, therefore, to maximize γ over b. In general, one would maximize over $k_\parallel$ as well, but we are restricting this study to long parallel wavelengths only. Of course, the saturated nonlinear response is not necessarily strongest at this wavelength. In addition, the allowed wave numbers in laboratory experiments[9,10] have physical restrictions via boundary conditions that affect the observed response. For these reasons, a comparison with any experiment must take into account the configuration of that experiment. It is not possible to prove conclusively that a global maximum has been found, but it is possible to locate local maxima over parameter space. In the present case, a single branch of the dispersion relation often has more than one locally (in b) maximum growth rate, as can be seen in the dashed line of Fig. 7. Each of these local maxima typically have different properties, as evidenced by their eigenfunctions (see, for example, Fig. 8). Figure 9 shows the locally maximum growth rate, $\gamma_{\max}$, as a function of separation, where each maximum is depicted with a different line style. Figure 10 shows the value of b for each local maximum, b_m, with the line styles corresponding to those in Fig. 9. The solid line is the mode with the strongest coupling (that is, where the eigenvalue is influenced by C_{12}); it also has the largest growth rate for this branch of the dispersion relation. The dotted and dashed lines represent modes that are perturbations of the single-layer dispersion (due to the variation of N). The single, wide layer behavior, shown as a thick solid

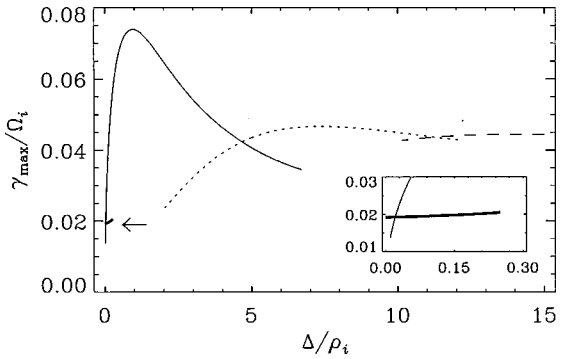

FIG. 9. Growth rate, maximized over b, for two identical layers as a function of separation Δ. The thicknesses are $L_1=L_2=3\rho_i$ and the flow velocities are $V_1=V_2=3\overline{v_i}$. The different line styles, solid, thick solid, dotted, and dashed, represent different local maxima. The wide layer maximum, the thick solid line, is marked with an arrow, and a close-up is shown in the inset.

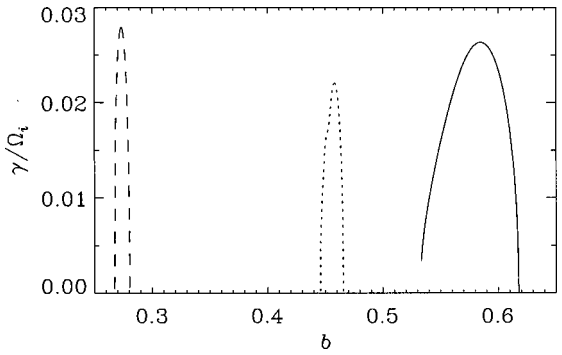

FIG. 11. Growth rate for oppositely directed flows as a function of b, corresponding to ground state eigenfunctions. The solid line is the single-layer mode (layer 1) perturbed by layer 2, while the dashed and dotted lines are new modes. The line styles correspond to Figs. 12–14. The parameters are $V_1=3\overline{v_i}$, $V_2=-1.8\overline{v_i}$, $L_1=L_2=3\rho_i$, and $\Delta=0$.

line marked by an arrow (with a close-up shown in the inset), only exists as a local maximum for extremely small values of the separation.

VI. OPPOSITELY DIRECTED FLOWS

The physics elucidated above suggests a second generic type of structure, that of oppositely directed flows. When V_1 is large enough, the wave energy density in layer 1 can be negative, leading to instability through coupling with the positive wave energy density outside the layer. This coupling also occurs if V_2 is allowed to be negative, forcing layer 2 to act as an energy sink, rather than an energy source. This type of profile, two adjacent flow layers with oppositely directed velocities, is commonly seen in the auroral ionosphere and is called a paired electrostatic shock.[2] Most importantly, the dispersion relation of this type of structure has many local maxima with widely varying frequencies and wave numbers, which can physically manifest itself as a broad spectrum.

We investigate the case where layer 1 has the same parameters as before, $V_1=3\overline{v_i}$ and $L_1=3\rho_i$. The second layer is adjacent to the first, $\Delta=0$, and has the same width, $L_2=L_1$, but has a flow velocity in the opposite direction, $V_2<0$. In this configuration, the growth rate can be a multiply peaked function of b, so that many local maxima exist. This situation is shown in Fig. 11, where the growth rate for $V_2=-1.8\overline{v_i}$ has three local maxima. All three of these roots correspond to the ground state eigenfunction. There also exist local maxima for other bound states, but for clarity we focus only on the ground state. As in the case of identical layers, the behavior of the maximum growth rates is the most physically interesting. Figures 12–14 show the locally maximized growth rate γ_{max}, frequency ω_r, and b_m for the four fastest growing roots, where b_m is the value of b for which $\gamma=\gamma_{max}$. Figure 15 shows the eigenfunctions of three of these roots for $V_2=-2.85\overline{v_i}$.

In Figs. 12–14, the solid lines represent the mode that is morphologically similar to the single-layer case (i.e., they are single-layer roots perturbed by the second layer). Its associated b_m is approximately 0.58 (compare with Fig. 2), its frequency is approximately $1.6\Omega_i$, and its growth rate is only slightly reduced from the single-layer case. Figure 15(a) shows the eigenfunction for this root, which exhibits the following behavior. To the left of layer 1, $x<-L_1/2$, the wave propagates. To the right of layer 2, $x>L_2+L_1/2$, the wave propagates but its amplitude is small because it had to tunnel

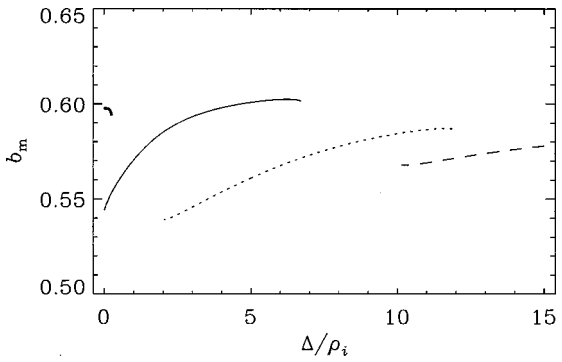

FIG. 10. Maximum value of b of four different local maxima for two identical layers as a function of separation Δ. The thicknesses are $L_1=L_2=3\rho_i$ and the flow velocities are $V_1=V_2=3\overline{v_i}$. The different line styles correspond to the growth rates shown in Fig. 9.

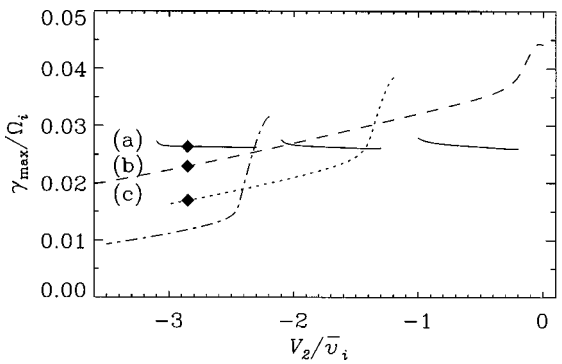

FIG. 12. Growth rates of four different local maxima for oppositely directed flows as a function of V_2. The solid line is the single-layer mode (layer 1) perturbed by layer 2, while the dashed, dotted, and dot-dashed lines are new modes. The parameters are $V_1=3\overline{v_i}$, $L_1=L_2=3\rho_i$, and $\Delta=0$. The three diamonds (a)–(c) mark eigenvalues for which the eigenfunctions are shown in Fig. 15.

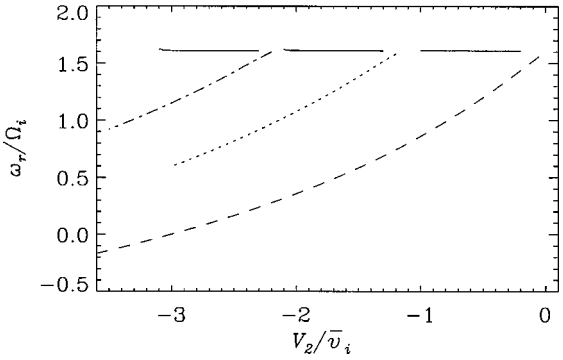

FIG. 13. Frequency of four different modes for oppositely directed flows as a function of V_2. The solid line is the single-layer mode (layer 1) perturbed by layer 2, while the dashed, dotted, and dot-dashed lines are new modes. The parameters are $V_1=3\bar{v}_i$, $L_1=L_2=3\rho_i$, and $\Delta=0$.

through layer 2 where the wave energy density is positive, which forces the eigenfunction to be evanescent. The effect of the presence of layer 2, with negative V_2, on this mode is minimal because the energy is still allowed to leave layer 1 (either by propagation on the left or absorption on the right), as required for a positive growth rate.

The other three roots (indicated by the dotted, dashed, and dot-dashed lines) are quite different in character and have no counterpart in the single-layer case. They have two properties that distinguish them from the single-layer case. First, they all exhibit the trend of decreasing ω_r, decreasing $\gamma_{\max}$, and decreasing b_{m} as $|V_2|$ increases (these quantities are all relatively constant for the single-layer case). In fact, for $|V_2|$ approximately equal to V_1 the frequency becomes extremely low, approaching $\omega_r\rightarrow 0$. Second, the eigenfunctions are not propagating waves, but are evanescent structures [see Figs. 15(b)–15(c)]. The flow profile thus modifies the usual ion Bernstein waves, which are coherent and narrow band, into a broadband (even static) response. At the same time, many modes become unstable, creating the possibility of both frequency and wavenumber spectra that are quite broad.

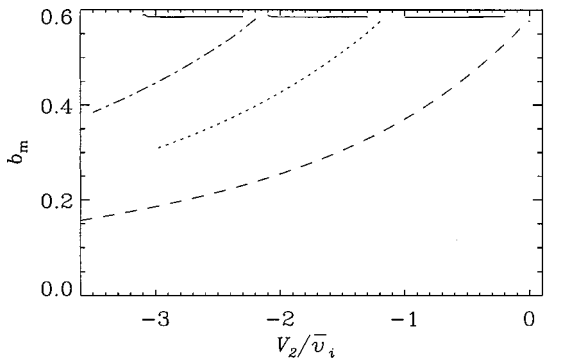

FIG. 14. Maximum value of b of four different modes for oppositely directed flows as a function of V_2. The solid line is the single-layer mode (layer 1) perturbed by layer 2, while the dashed, dotted, and dot-dashed lines are new modes. The parameters are $V_1=3\bar{v}_i$, $L_1=L_2=3\rho_i$, and $\Delta=0$.

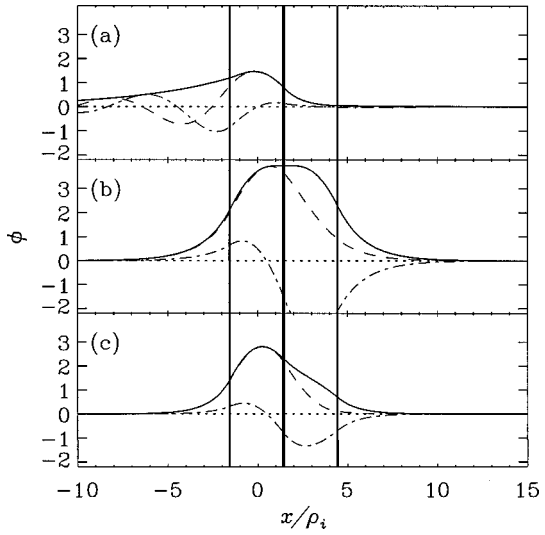

FIG. 15. Eigenfunctions of three different modes for oppositely directed flows for $V_2=-2.85$, with the labels corresponding to the diamonds in Fig. 12. The dashed line is Re ϕ, the dot-dashed line is Im ϕ, and the solid line is $|\phi|$. The other parameters are $V_1=3\bar{v}_i$, $L_1=L_2=3\rho_i$, and $\Delta=0$. The vertical lines delineate the edges of the layers, and the dotted lines mark the zero values.

VII. CONCLUSION

Structure in the perpendicular flow profile of a plasma, in the form of layers flowing in the same direction or in opposite directions, enriches its instability properties. Profiles similar to those investigated here are observed, for example, in the auroral ionosphere.

Two important conclusions follow from this work. First, instabilities due to a nonuniform velocity are quite robust to the inclusion of fine structure in the flow profile. In fact, the fine structure can even be destabilizing (i.e., when two layers are close and the coupling is strong). We do not expect this conclusion to be altered qualitatively if further structure (three or more layers, for example) is added to the flow profile, although a determination of the quantitative aspects of the interaction require numerical analysis. Second, when oppositely directed flows exist, extremely low-frequency waves become unstable, with associated evanescent field structures. This quasistatic response is similar to that which is observed in the auroral ionosphere.[2] In addition to the possibility of low frequencies, many modes become unstable, which could result in a broad frequency spectrum for $\omega\lesssim\omega_{ci}$ and a broad wave number spectrum for $k_\perp\rho_i\lesssim 1$.

The two generic velocity profiles investigated here were chosen for their similarity to profiles observed by sounding rockets and satellites.[1–4] For this reason, these results are intended to shed light on the current understanding of the process of wave generation in the auroral ionosphere.

ACKNOWLEDGMENTS

We would like to thank W. E. Amatucci, J. J. Carroll, V. V. Gavrishchaka, M. E. Koepke, and J. R. Peñano for numerous useful discussions and for critically reading the

manuscript. We would also like to thank the referee for extremely useful comments that improved the quality of the presentation.

This work was sponsored by the Office of Naval Research and the National Aeronautics and Space Administration.

APPENDIX: DISPERSION RELATION

When the flow velocity is piecewise constant, the second-order differential equation for ϕ is mathematically identical to the quantum square well problem. The simplest case, a single flow layer or a single square well, is covered in most textbooks on quantum mechanics.[17] In this appendix, we solve the eigenvalue equation for two layers, and extend the solution to an arbitrary number of layers. The boundary conditions are written in matrix form, and we show that they can be built from two types of submatrices; those that represent the dispersion relation of each layer separately, and those that represent the coupling between the layers. In this way, the dispersion relation for any number of flow layers (or square wells) can be determined, with the coupling explicitly shown.

Equation (2) can be rewritten as

$$\left\{\frac{\partial^2}{\partial x^2}+\mathsf{k}^2(x)\right\}\phi(x)=0, \tag{A1}$$

where $\mathsf{k}^2(x)$ is the effective potential. In each region listed in Eq. (4), the potential ϕ is expressed as a sum of both right-going and left-going plane waves with arbitrary amplitudes (except for the outermost regions, where only outgoing plane waves satisfy the correct boundary conditions as $x\rightarrow\pm\infty$)

$$\phi=\left\{\begin{array}{ccc} & & \varphi_1 e^{-i\mathsf{k}_0 x} \\ \varphi_2 e^{+i\mathsf{k}_1 x} & + & \varphi_3 e^{-i\mathsf{k}_1 x} \\ \varphi_4 e^{+i\mathsf{k}_0 x} & + & \varphi_5 e^{-i\mathsf{k}_0 x} \\ \varphi_6 e^{+i\mathsf{k}_2 x} & + & \varphi_7 e^{-i\mathsf{k}_2 x} \\ \varphi_8 e^{+i\mathsf{k}_0 x} & & \end{array}\right\}, \tag{A2}$$

where $\mathrm{Im}\,\mathsf{k}_0>0$. Because the system is uniform in both the y and z directions, ϕ must be continuous across each boundary. Integrating Eq. (A1) across each boundary results in the condition that $\partial\phi/\partial x$ must also be continuous. These are the usual quantum-mechanical boundary conditions that determine the amplitudes φ_i. The two matching conditions applied to each of the four boundaries result in a set of eight coupled equations for the amplitude of ϕ, which can be written as a matrix equation

$$\mathsf{M}\cdot\boldsymbol{\varphi}=0, \tag{A3}$$

where $\boldsymbol{\varphi}=\{\varphi_1,\varphi_2,\varphi_3,\varphi_4,\varphi_5,\varphi_6,\varphi_7,\varphi_8\}$ and M is the matrix of coefficients. Setting the determinant of M equal to zero gives the dispersion relation

$$\det\mathsf{M}=D_{12}^{(2)}=0. \tag{A4}$$

The form of $D_{12}^{(2)}$ is shown explicitly in Eq. (5). The matrix M is neither symmetrical nor does it display the coupling clearly. However, it can be written to explicitly show the symmetry and coupling between the two layers clearly if it first is transformed by a matrix T (shown below), which eliminates unimportant phase factors, and then is written as a 2×2 matrix of 4×4 submatrices. This gives a new matrix $\bar{\mathsf{M}}$

$$\bar{\mathsf{M}}\equiv\mathsf{M}\cdot\mathsf{T}=\begin{bmatrix}\mathsf{M}_1 & \mathsf{C}_\Delta^U\\ \mathsf{C}_\Delta^L & \mathsf{M}_2\end{bmatrix}, \tag{A5}$$

where M_1 is the 4×4 matrix which gives the single-layer dispersion relation for layer 1,

$$\mathsf{M}_1=\begin{bmatrix} 1 & -1/m_1 & -m_1 & 0\\ -\mathsf{k}_0 & -\mathsf{k}_1/m_1 & \mathsf{k}_1 m_1 & 0\\ 0 & -\mathsf{k}_1 m_1 & \mathsf{k}_1/m_1 & \mathsf{k}_0\\ 0 & -m_1 & -1/m_1 & 1\end{bmatrix}, \tag{A6}$$

and the matrix elements are given by $m_1=\exp(i\mathsf{k}_1 L_1/2)$, where k_1 is the wave number in layer 1 and L_1 is the width of layer 1. That is, $\det\mathsf{M}_1=D_1^{(1)}$, which is shown explicitly in Eqs. (6) and (8). Equivalently, for the second layer, $\det\mathsf{M}_2=D_2^{(1)}$. The upper and lower off-diagonal submatrices, C^U and C^L, couple the two layers,

$$\mathsf{C}_\Delta^U=\begin{bmatrix} 0 & 0 & 0 & 0\\ 0 & 0 & 0 & 0\\ -\mathsf{k}_0 e^{i\mathsf{k}_0\Delta} & 0 & 0 & 0\\ e^{i\mathsf{k}_0\Delta} & 0 & 0 & 0\end{bmatrix}, \tag{A7}$$

$$\mathsf{C}_\Delta^L=\begin{bmatrix} 0 & 0 & 0 & e^{i\mathsf{k}_0\Delta}\\ 0 & 0 & 0 & \mathsf{k}_0 e^{i\mathsf{k}_0\Delta}\\ 0 & 0 & 0 & 0\\ 0 & 0 & 0 & 0\end{bmatrix}, \tag{A8}$$

where Δ is the separation between the two layers. The transformation matrix T can also be written in the matrix-of-matrices format, as a product of two matrices

$$\mathsf{T}=\begin{bmatrix}\mathsf{I} & \mathsf{O}\\ \mathsf{O} & \mathsf{T}_{12}\end{bmatrix}\cdot\begin{bmatrix}\mathsf{T}_1 & \mathsf{O}\\ \mathsf{O} & \mathsf{T}_2\end{bmatrix}, \tag{A9}$$

where I and O are the 4×4 unit matrix and zero matrix, respectively,

$$\mathsf{T}_{12}=\begin{bmatrix} e^{+i\mathsf{k}_0 d} & 0 & 0 & 0\\ 0 & e^{-i\mathsf{k}_2 d} & 0 & 0\\ 0 & 0 & e^{+i\mathsf{k}_2 d} & 0\\ 0 & 0 & 0 & e^{-i\mathsf{k}_0 d}\end{bmatrix}, \tag{A10}$$

$d=\Delta+L_1/2+L_2/2$ is the distance between the centers of each layer, and

$$\mathsf{T}_1=\begin{bmatrix} e^{-i\mathsf{k}_0 L_1/2} & 0 & 0 & 0\\ 0 & 1 & 0 & 0\\ 0 & 0 & 1 & 0\\ 0 & 0 & 0 & e^{-i\mathsf{k}_0 L_1/2}\end{bmatrix}. \tag{A11}$$

The submatrix T_{12} effectively translates layer 2 a distance $-d$ along the x axis so that it is centered on the origin, and the submatrix T_1 effectively translates the boundaries of layer 1 to the origin (and T_2 makes a similar translation for

layer 2). These translations eliminate the phase factors associated with the fact that the boundaries between the different regions are not located at the origin, and put $\bar{\mathsf{M}}$ in a symmetric form. Because $\det \mathsf{T} = \exp\{-i\mathsf{k}_0(L_1+L_2)\}$, the determinants of M and $\bar{\mathsf{M}}$ differ only by an unimportant phase factor, and either may be used to calculate the dispersion relation. A calculation of the eigenfunctions, however, requires the use of M, because it includes the proper phase factors.

The generalization of $\bar{\mathsf{M}}$ to an arbitrary number of layers is simple because the inherent symmetry is clear and the coupling is explicit. The result for N layers is a block tridiagonal matrix

$$\bar{\mathsf{M}}^{(N)} = \begin{bmatrix} \mathsf{M}_1 & \mathsf{C}^U_{\Delta_1} & \mathsf{O} & \cdots & \mathsf{O} \\ \mathsf{C}^L_{\Delta_1} & \mathsf{M}_2 & \mathsf{C}^U_{\Delta_2} & \cdots & \mathsf{O} \\ \mathsf{O} & \mathsf{C}^L_{\Delta_2} & \mathsf{M}_3 & \cdots & \mathsf{O} \\ \vdots & \vdots & \vdots & \ddots & \mathsf{C}^U_{\Delta_{N-1}} \\ \mathsf{O} & \mathsf{O} & \mathsf{O} & \mathsf{C}^L_{\Delta_{N-1}} & \mathsf{M}_N \end{bmatrix}, \tag{A12}$$

where Δ_i is the separation between the layer i and layer $i+1$. The transformation matrix T has a similar extension to N layers

$$\mathsf{T}^{(N)} = \begin{bmatrix} \mathsf{I} & \mathsf{O} & \cdots & \mathsf{O} \\ \mathsf{O} & \mathsf{T}_{12} & \cdots & \mathsf{O} \\ \vdots & \vdots & \ddots & \mathsf{O} \\ \mathsf{O} & \mathsf{O} & \mathsf{O} & \mathsf{T}_{1N} \end{bmatrix} \cdot \begin{bmatrix} \mathsf{T}_1 & \mathsf{O} & \cdots & \mathsf{O} \\ \mathsf{O} & \mathsf{T}_2 & \cdots & \mathsf{O} \\ \vdots & \vdots & \ddots & \mathsf{O} \\ \mathsf{O} & \mathsf{O} & \mathsf{O} & \mathsf{T}_N \end{bmatrix}, \tag{A13}$$

where T_{1i} is a 4×4 submatrix that translates layer i to the origin, T_j is a 4×4 submatrix that translates the boundaries of layer j to the origin, and I and O are the 4×4 identity and zero submatrices defined earlier. The dimensions of $\bar{\mathsf{M}}^{(N)}$ and $\mathsf{T}^{(N)}$ are thus $4N\times4N$, and the equation $\det \bar{\mathsf{M}}^{(N)} = 0$ is the dispersion relation for N layers of width L_i and separation Δ_i. From the system of equations contained in $\bar{\mathsf{M}}^{(N)} \cdot \mathsf{T}^{(N)} \cdot \boldsymbol{\varphi} = 0$, and a knowledge of the eigenvalues, the eigenfunctions may be calculated.

Interest in the multiple square well problem has also recently surged in the condensed matter community due to advances in manufacturing semiconductor heterostructures, which are layers of semiconductor materials with different band gaps.[18,19] The different band gaps result in a one-dimensional, piecewise-constant electric potential. The technique that is used to solve for the eigenvalues and eigenfunctions of such a potential structure is the transfer matrix method,[20] which evaluates a product of 2×2 matrices (one for each boundary); the dispersion relation is then found by forcing the incoming waves to have zero amplitude.[18,19] It is a different, albeit equivalent, approach to that taken in this appendix. (The boundary condition on $\partial\phi/\partial x$ must be modified in semiconductors, however, depending on the specific excitation of interest.[20]) The specific case of two, asymmetric wells has also been investigated,[21] although in semiconductors the interest is in the tunneling of electrons between the two wells.

[1] F. S. Mozer, R. Ergun, M. Temerin, C. Cattell, J. Dombeck, and J. Wygant, Phys. Rev. Lett. **79**, 1281 (1997).
[2] F. S. Mozer, C. W. Carlson, M. K. Hudson, R. B. Torbert, B. Parady, J. Yatteau, and M. C. Kelley, Phys. Rev. Lett. **38**, 292 (1977).
[3] P. M. Kintner, J. Bonnell, R. Arnoldy, K. Lynch, C. Pollock, and T. Moore, Geophys. Res. Lett. **23**, 1873 (1996).
[4] J. Bonnell, EOS Trans. Am. Geophys. Union **78**, Fall Meet. Suppl. F612 (1997).
[5] M. E. Koepke, J. J. Carroll III, M. Zintl, C. A. Selcher, and V. Gavrishchaka, Phys. Rev. Lett. **80**, 1441 (1998).
[6] M. E. Koepke, J. J. Carroll III, and M. Zintl, Phys. Plasmas **5** 1671 (1998).
[7] G. Ganguli, Y. C. Lee, and P. Palmadesso, Phys. Fluids **28**, 761 (1985).
[8] G. Ganguli, Phys. Plasmas **4**, 1544 (1997).
[9] M. E. Koepke, W. E. Amatucci, J. J. Carroll III, and T. E. Sheridan, Phys. Rev. Lett. **72**, 3355 (1994).
[10] W. E. Amatucci, D. N. Walker, G. Ganguli, J. A. Antoniades, D. Duncan, J. H. Bowles, V. Gavrishchaka, and M. E. Koepke, Phys. Rev. Lett. **77**, 1978 (1996).
[11] P. Palmadesso, G. Ganguli, and Y. C. Lee, in *Ion Acceleration in the Magnetosphere and Ionosphere*, edited by T. Chang (American Geophysical Union, Washington, D.C., 1986), p. 301.
[12] L. N. Trefethen, A. E. Trefethen, S. C. Reddy, and T. A. Driscoll, Science **261**, 578 (1993).
[13] I. B. Bernstein, Phys. Rev. **109**, 10 (1958).
[14] J. P. M. Schmitt, Phys. Rev. Lett. **16**, 982 (1973).
[15] G. Ganguli, Y. C. Lee, and P. Palmadesso, Phys. Fluids **31**, 823 (1988).
[16] V. V. Gavrishchaka, G. I. Ganguli, P. M. Bakshi, and M. E. Koepke, Phys. Plasmas **5**, 10 (1998).
[17] L. I. Schiff, *Quantum Mechanics*, 3rd ed. (McGraw–Hill, New York, 1968), pp. 37–44.
[18] R. M. Kolbas and N. Holonyak Jr., Am. J. Phys. **52**, 431 (1984).
[19] R. T. Deck and X. Li, Am. J. Phys. **63**, 920 (1995).
[20] S. G. Yu, K. W. Kim, M. A. Stroscio, G. J. Iafrate, J.-P. Sun, and G. I. Haddad, J. Appl. Phys. **82**, 3363 (1997).
[21] S. Ten, F. Henneberger, M. Rabe, and N. Peyghambarian, Phys. Rev. B **53**, 12 637 (1996).